

Review

Carbons Formed in Methane Thermal and Thermocatalytic Decomposition Processes: Properties and Applications

Emmi Välimäki¹, Lasse Yli-Varo¹, Henrik Romar² and Ulla Lassi^{1,*} 

¹ Research Unit of Sustainable Chemistry, University of Oulu, P.O. Box 4300, FI-90014 Oulu, Finland; emmi.valimaki@oulu.fi (E.V.); lasse.yli-varo@oulu.fi (L.Y.-V.)

² Hycamite TCD Technologies Ltd., FI-67100 Kokkola, Finland; henrik.romar@hycamite.com

* Correspondence: ulla.lassi@oulu.fi; Tel.: +358-400294090

Abstract: The hydrogen economy will play a key role in future energy systems. Several thermal and catalytic methods for hydrogen production have been presented. In this review, methane thermocatalytic and thermal decomposition into hydrogen gas and solid carbon are considered. These processes, known as the thermal decomposition of methane (TDM) and thermocatalytic decomposition (TCD) of methane, respectively, appear to have the greatest potential for hydrogen production. In particular, the focus is on the different types and properties of carbons formed during the decomposition processes. The applications for carbons are also investigated.

Keywords: methane; hydrogen; carbon; catalytic decomposition; wet decomposition; dry decomposition; hydrogen economy



Citation: Välimäki, E.; Yli-Varo, L.; Romar, H.; Lassi, U. Carbons Formed in Methane Thermal and Thermocatalytic Decomposition Processes: Properties and Applications. *C* **2021**, *7*, 50. <https://doi.org/10.3390/c7030050>

Academic Editor: Gil Goncalves

Received: 4 June 2021

Accepted: 23 June 2021

Published: 25 June 2021

Publisher's Note: MDPI stays neutral with regard to jurisdictional claims in published maps and institutional affiliations.



Copyright: © 2021 by the authors. Licensee MDPI, Basel, Switzerland. This article is an open access article distributed under the terms and conditions of the Creative Commons Attribution (CC BY) license (<https://creativecommons.org/licenses/by/4.0/>).

1. Introduction

The hydrogen economy has attracted a significant amount of interest since the European Union (EU) revealed a new strategy to reach carbon neutrality by 2050. The increased interest in hydrogen is due to its potential as a fuel and as an energy carrier, its capability for energy storage, and its use as a carbon-neutral feedstock without carbon dioxide (CO₂) emissions. At present, hydrogen is mainly produced from fossil fuels, and hydrogen production in the EU releases about 70 to 100 million tons of CO₂ per annum [1]. If a means of production can be developed that does not release CO₂, hydrogen will play a key role in creating a climate-neutral Europe. One major issue to be resolved is how to make the CO₂-free hydrogen production process cost competitive compared with fossil-based hydrogen processes.

Production of hydrogen from methane is considered to be the best option compared to the use of other hydrocarbons. This is due to the fact that methane is abundant, and can be easily transported and stored when needed. Methane also has a high hydrogen to carbon ratio of 4:1 [2]. In addition to methane's significant importance in hydrogen production, methane is also used in power generation and methanol production [3]. Hydrogen can be produced from methane in several ways. In this article, we present the most important production processes and note some advantages and disadvantages for each process. At present, the most commonly used processes for hydrogen production from methane, and especially renewable biomethane, are steam methane reforming (SMR), dry methane reforming (DMR), and partial oxidation (PO) [4]. None of these processes are CO₂-neutral; CO₂ is emitted, or a separate carbon capture process is required after the main process. The addition of the extra step increases the price of the hydrogen produced. In the thermal decomposition of methane (TDM) and thermocatalytic decomposition (TCD) of methane, no oxygen is involved in the reaction, and solid carbon is formed. Compared to other methane conversion methods in which carbon is released to the atmosphere, TDM and TCD processes create carbon capture and therefore have a significant effect on carbon's neutrality and footprint. Most of the recently published papers consider the formation

and use of the hydrogen formed in the decomposition of methane, whereas the carbons formed in the process are considered as less important. However, the carbon formed has its own markets and possible applications, such as usage in water purification and energy storage applications. A full use of the carbons formed in the TDM and TCD processes in potential applications would result in increased value, and increase the profitability of these decomposition processes and the overall hydrogen economy. In this paper, we focus on the carbon produced from the TCD process, its properties, and possible applications. We also briefly examine other methane conversion processes to highlight the benefits of TCD.

2. Production Methods for Hydrogen and Carbon from Methane

Various methods exist for producing hydrogen from methane, such as SMR, DRM, PO, TDM, and TCD. The latter two processes are considered more environmentally friendly because they do not create CO₂ or carbon monoxide (CO) emissions [5]. One important difference between these methods is the end use of the carbon. In the first three reactions (SMR, DRM, and PO), carbon is emitted as CO₂ or CO, whereas in TDM and TCD, solid deposits of carbon are formed. Instead of producing CO₂ gas, TDM/TCD processes produce carbon as a potentially valuable solid. The reactions for these processes and corresponding reaction enthalpies are presented in Table 1.

Table 1. Chemical reactions for hydrogen production from methane and corresponding reaction enthalpies. In the first three reactions (SMR, DRM, and PO), carbon is emitted as CO₂ or CO, whereas in TDM and TCD, solid deposits of carbon are formed.

Production Method	Chemical Equation	Reaction Enthalpies	Equation Number
Steam methane reforming (SMR)	$\text{CH}_4 + \text{H}_2\text{O} \rightarrow \text{CO} + 3\text{H}_2$	$\Delta H_{298\text{K}} = 206 \text{ kJ/mol}$	(1)
Water gas shift reaction (WGS)	$\text{CO} + \text{H}_2\text{O} \rightarrow \text{CO}_2 + \text{H}_2$	$\Delta H_{298\text{K}} = -41 \text{ kJ/mol}$	(2)
Dry reforming of methane (DRM)	$\text{CH}_4 + \text{CO}_2 \rightarrow 2\text{CO} + 2\text{H}_2$	$\Delta H_{298\text{K}} = 247 \text{ kJ/mol}$	(3)
Partial oxidation (PO)	$\text{CH}_4 + 0.5\text{O}_2 \rightarrow \text{CO} + 2\text{H}_2$	$\Delta H_{298\text{K}} = -23 \text{ kJ/mol}$	(4)
Thermal decomposition of methane (TDM)	$\text{CH}_4 \rightarrow \text{C} + 2\text{H}_2$	$\Delta H_{298\text{K}} = 75 \text{ kJ/mol}$	(5)
Thermocatalytic decomposition of methane (TCD)			

SMR (Equation (1)) is one of the most mature processes in hydrogen production, starting from methane. The SMR reaction is endothermic and therefore has a high energy consumption. However, the SMR process has some severe drawbacks and challenges that should be considered. The process is usually carried out at relatively high temperatures, 973–1273 K, and at reaction pressures ranging from 0.3 to 2.5 MPa [6]. Another drawback is that SMR generates large amounts of CO₂ [5]. According to Soltani et al. [7], SMR generates approximately 7 kg of CO₂ to every 1 kg of H₂ produced. Although SMR is one of the least expensive processes in large-scale hydrogen production [6], a harsh reaction environment can create corrosion risks, especially if sulfur is present, a condition that can appear if the gas is not adequately purified [6,8]. In SMR, the catalyst plays a key role in the process. The use of a catalyst increases the yield of hydrogen and lowers the temperature, and no pressure is used. The cost of the catalysts, possible toxicity of the active metals used, and availability and deactivation of the catalyst by the formation of coke, should be considered [4,9]. To gain additional hydrogen from the SMR process, the water gas shift (WGS) reaction (Equation (2)) is usually introduced. In the WGS, CO is transformed into CO₂ and hydrogen, usually after the SMR reaction [9]. WGS is an exothermic reaction that is normally undertaken in two reactors: one with a high temperature in which thermal equilibrium is reached and one with a lower temperature in which the catalyst provides higher conversions; that latter process is much slower. In addition to SMR, WGS is also affected by process parameters, and therefore the variation in performance can vary. Another drawback of WGS is that the activity of the reaction decreases at lower temperatures, which creates additional carbon. This can be an issue, especially in fuel cell applications where lower CO is required.

Another well-known hydrogen production process is dry reforming (Equation (3)). One of the main benefits of DRM is that it consumes methane and CO₂ to create hydrogen, and it is also cheaper when compared with SMR and PO [6]. However, like SMR, it produces CO [9]. The operating temperature ranges from 923 to 1123 K, and the pressure is normally 0.1 MPa [6].

PO is an exothermic reaction (Equation (4)) carried out at a pressure of 10 MPa and a temperature range of 1223 to 1373 K [4,10]. Due to the exothermic reaction, the process is difficult to control because of the induced hotspots on the catalyst [8]. If air is used as an oxygen source, nitrogen separation is required from the gas prior to the reaction, a process that increases operational costs. It is therefore recommended to use pure oxygen and/or separate the oxygen from the air [10]. Oxygen separation from air makes the process costly [4]. The benefits of the process are short residence time, high conversion rates, high selectivity of syngas, good economic conversion, and compactness [8,11–13].

Thermal decomposition of methane has two alternating routes (Equation (5)): catalytic (TCD) and non-catalytic (TDM) [14]. The latter has been used for several decades for the production of carbon black. Methane is one of the most stable hydrocarbons due to its very strong carbon–hydrogen bond and high molecular structure symmetry [15]. In TDM, the reaction temperature is relatively high, and may reach 1473 K for a reasonable hydrogen yield [14,15]. By using a catalyst, this temperature can be significantly lowered, and the catalyst can influence the formed carbon. Both processes are CO₂-free, and therefore they have gained increased interest. In this paper, however, we focus on the TCD catalytic reaction, because the carbon formed can have different morphologies and greater value than with the use of TDM. TCD has remained in the laboratory phase mostly because of the deactivation of the catalyst, the possibility of CO₂ formation during reactivation of the catalyst, and the unreacted methane in hydrogen [15]. Several catalysts have been tested for the reaction, and these can be divided into two separate groups: noble metals and transition metals, such as nickel and iron; and carbon-based materials, such as activated carbon [16]. Metal catalysts can be supported by high surface area materials, such as Al₂O₃ and SiO₂, and carbon can be doped with some metals. Different catalysts have varying effects on the process, and so it is important to select the best catalyst to produce carbon. The effect of catalysts is discussed later in this paper. Economic and environmental issues should also be considered.

In the TCD process, the methane molecules decompose on the surface of the catalytic metals, and in the crevices or cracks of the catalyst. The reaction generates hydrogen molecules and carbon atoms. Carbon diffuses to the metal and accumulates to form carbon deposits [17,18]. In TCD, amorphous, graphitic, and carbon nanotube (CNT) morphologies of carbon can be found, and the process parameters affect the morphology of the carbon. The reaction temperature is above 1473 K, and the carbon formed is mainly amorphous [16]. The CNTs' growth mechanism can be divided into two types, tip growth and base growth, in which one or the other is active, depending on the interaction between catalyst metal and support weakness. Weak interaction leads to tip growth, in which the catalyst particle is lifted by the growing CNT. Strong supports lead to base growth, in which the growth mechanism proceeds through an open tip. Regardless of the manner in which the carbon grows on the catalyst, one of the main problems to be resolved is the separation of the carbon and catalyst used without generating any CO₂ emissions [19]. The size of the catalyst particle can affect the growth of the carbon in TCD process. This is schematically shown in Figure 1, in which the possible effect of large and small nickel catalyst particles on the growth of carbon is shown. Large nickel particles induce more tip growth of carbon, whereas, in the case of small nickel particles, carbon grows on the catalyst particle and encapsulates it.

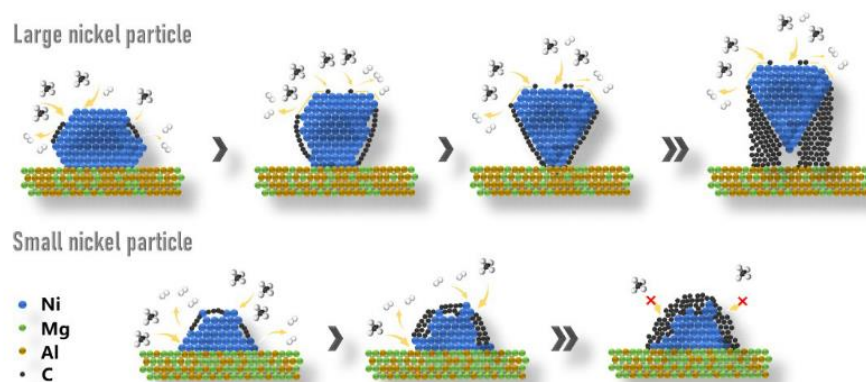


Figure 1. Possible mechanisms of carbon growth in the presence of large and small nickel particles [18]. Large nickel particles induce tip growth of carbon, whereas, in the case of small nickel particles, carbon grows on the catalyst particle and encapsulates it.

3. Carbon Morphologies

Carbon is a polymorphic material; it can exist in more than one form, such as diamond, graphite, and fullerene (also known as carbon nano-onions (CNOs) and CNTs). Its morphologies are shown in Figure 2. In addition, the level of crystallinity varies; carbon can have amorphous, turbostratic, and graphitic crystallinity [20]. Graphite has a crystal structure that is composed of carbon atoms hexagonally arranged in layers. Each carbon atom has a strong covalent bond among three neighboring atoms, and the fourth electron can form a weak bond between layers, which allows these layers to be separated. These increase, for example, the lubricant properties of graphite. In addition, the hexagonal sheets have relatively high electrical conductivity.

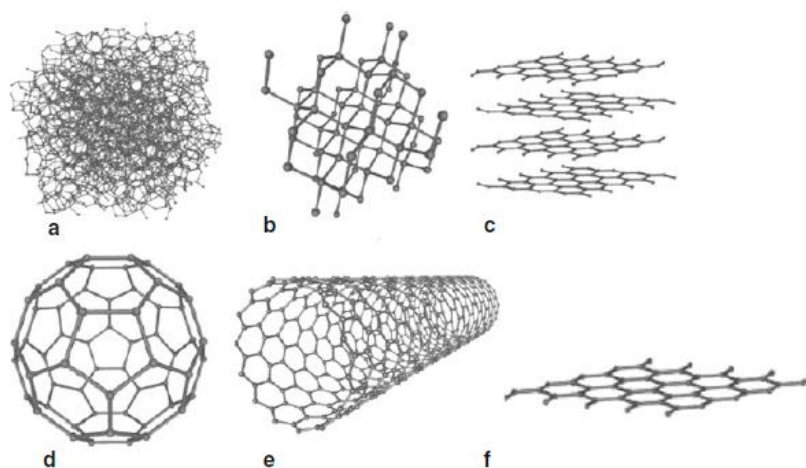


Figure 2. Structures of various carbon morphologies: (a) amorphous carbon, (b) diamond, (c) graphite, (d) fullerene, (e) carbon nanotube (CNT), and (f) graphene [21]. Adapted with permission from [21]. Springer Nature, 2011.

The structure, texture, and morphologies of the carbons formed in the TCD reaction depend on the reaction conditions, such as pressure, temperature, catalysts, and gas phase composition. These properties make them suitable for many applications. The properties that affect applicability, and are thus of common interest, are surface area, pore volume, pore size, porosity, and surface chemistry, in addition to the morphology [22]. Transmission electron microscopy (TEM) and scanning electron microscopy (SEM) are used to study the length, thickness, morphology, impurities, and topography of carbon deposits. Thermogravimetric analysis (TGA) is used to quantify the amount of the deposits and the

thermal stability of the specimen. Specific surface area is measured according to the theory of Brunauer–Emmett–Teller, commonly called BET analysis. X-ray diffraction (XRD) is used to create diffractograms of the deposits, and the crystallinity, phase structure, and purity of the specimen can be obtained from XRD. Figure 3 shows XRD patterns for carbons produced by the TCD process using three different nickel catalysts. XRD peaks indicate the crystal structure of materials. In Figure 3, the pink circle indicates carbon morphology, which, in this case, is graphite for all produced carbons. Raman spectra can also be used to determine purity, crystallinity, and degree of structural disorder, for example, the defects and tube alignment of the CNT [23–26].

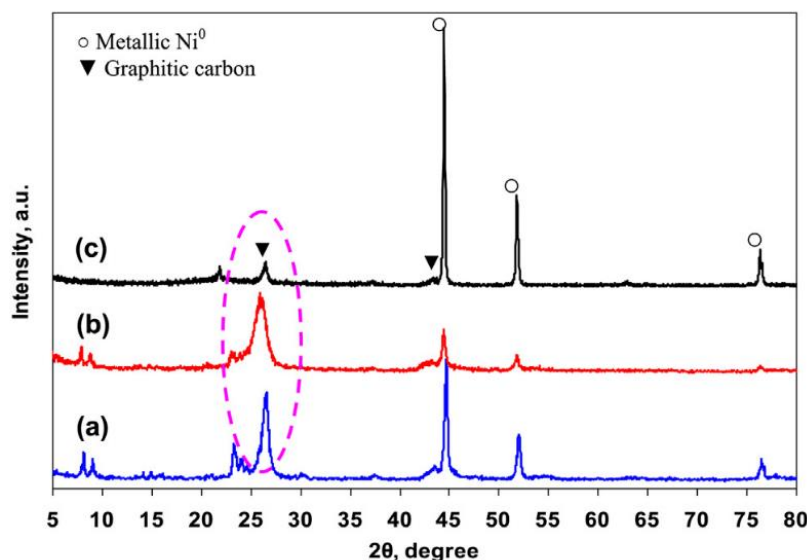


Figure 3. XRD patterns for carbon materials produced by the TCD process over reduced (a) Ni/Z-25, (b) Ni/Z-400, and (c) Ni/AS catalysts [27]. In all cases, a graphite-like carbon crystal structure is seen. Adapted with permission from [27]. Elsevier, 2016.

One of the most studied components in the TCD process to produce carbon are CNTs. These are rolled graphene layers that can form single- or multiwalled tubes, which can differ in thickness, diameter, and layer amount [28]. Typical properties of CNTs are high electrical conductivity and high tensile strength. Physically and chemically, CNTs are stable [29]. They are used in polymers, wastewater/pollution treatment, conductive paints/coatings, biosensors, electronics, energy storage, and environmental applications [29,30]. A major application is to reinforce polymers to improve thermal, electrical, and mechanical properties, and interest in using CNTs in the production of lithium-ion batteries has increased, because they improve the efficiency of the batteries [30].

Carbon fibers (CNFs) are polycrystalline; they have both graphitic and amorphous regions. The amorphous regions lack hexagonal carbon networks that are characteristic of graphite [20]. CNFs have high tensile strength and stiffness, and low density and coefficient of thermal expansion. They are used in the aerospace, vehicle manufacturing, energy, sports equipment, and chemical and textile industries, and as a reinforcement in composite materials [30].

Carbon fullerenes resemble the shape of a sphere [20]. One form of carbon fullerenes is commonly referred to as a CNO, which are multiwalled fullerenes [31]. Carbon fullerenes have not been found in the TCD reaction, but CNOs have. Fullerenes have shown significant promise in several applications, such as solid lubrication, electromagnetic shielding, fuel cells, heterogeneous catalysis, energy storage, electro-optical devices, and supercapacitors [32]. CNOs can have a crucial effect on the TCD process. According to the investigations of Zhou et al. [19], formed CNOs encapsulated the catalyst and, therefore, the catalyst was deactivated.

4. Process Parameters Affecting the Properties of Carbon in TDM and TCD Processes

As mentioned previously, the TCD of methane produces hydrogen and carbon. The yields and carbon morphology are dependent on various process parameters, such as the kind of catalyst used, size of the catalyst's metal particle, promoter material, reaction temperature, pressure, and gas hourly space velocity (GHSV) [33–40]. According to Li et al. [40], the carbon yield is mostly affected by the particle size of the metallic catalyst, and also affects the catalytic life [41]. It has also been mentioned that the carbon morphology affects the efficiency of thermocatalytic decomposition when carbon is used as a catalyst support [35]. The factors affecting catalytic life have been widely studied, and it is valuable to understand how this occurs and the kind of carbon that is formed. In the TDM process, temperatures are higher than those in TCD, and are typically above 1200 °C. The main products in TDM are carbon black graphite-like carbon and coke [42].

4.1. Effect of Catalyst and Promoters on the Carbon Amount and Quality

Guil-Lopez et al. [43] compared metal and carbon catalysts in the TCD process, and their differences in terms of hydrogen production and carbon morphology (size and shape). They used Ni and Fe metal catalysts with different supports and six different carbon catalysts, which included carbon black, activated carbon, graphene, and CNTs. Interest in carbon catalysts has risen due to their lower cost, higher temperatures, which affect the methane conversion rate, and the possibility that there is no need to separate catalyst carbon and produced carbon [16]. According to the results of a study by Guil-Lopez et al. [43], metal catalysts are more prone to produce CNTs when carbon catalysts produced more graphene-like carbon. Carbon catalyst activity depends on the chemical structure, such as defects, BET surface area, and pore volume. By designing and preparing carbon materials with specific pore systems, catalytic activity and stability can be improved [22]. When comparing amorphous carbon with more ordered carbon, Muradov found that amorphous carbon had more catalytic activity than ordered carbon [44].

Nickel-based catalysts have gained interest due to their capability to produce high-value carbon, such as CNTs and CNFs, and because of their high catalytic activity [45]. The drawbacks of using Ni catalysts are their sensitivity to the operation temperature and quick deactivation [46]. Torres et al. [36] studied the effect of numerous catalysts on TCD and found that the Cu-doped Ni/Al₂O₃ catalyst had a higher yield in carbon formation and a longer activity time at a temperature range of 823–873 K. In addition, the bimetallic Ni-Cu catalyst produced shorter carbon filaments, and the diameter of the filament was more constant compared with the metallic catalyst. Saraswat and Pant [38] studied Cu/Zn metals as promoters with a Ni aluminosilicate catalyst in TCD. Their results indicate that the yield and type of carbon depends on the added amount of Cu and Zn promoters, in addition to the process temperature. Saraswat et al. [47] studied the effect of the process parameters on the methane conversion and carbon amount. First, they studied the effect of temperature on yield. They examined the process at five different temperatures, ranging from 823 to 1023 K in 323 degree steps. The best methane conversion rate was found at 1023 K. In further studies, they used this temperature. The highest carbon yields were at 1023 K and with the catalyst combination of 50% Ni–10% Cu with the support of SiO₂. The carbon yield using this 50% Ni–10% Cu/SiO₂ catalyst was 710%. The second highest carbon yield (610%) was obtained using the 50% Ni–5% Cu catalyst. Table 2 presents the results of Saraswat et al. [46], indicating the catalyst and support used, temperature and GHSV of the TCD process, and the produced carbon amounts and yields. Bai et al. [33] tested active CNFs as catalysts that were loaded with Ni. They stated that the surface structure and textural properties of the CNFs can affect the stability and activity of the catalyst. Their produced carbon was consistent in diameter and relatively long. Nickel particle size has been proven to have a significant effect on carbon formation and catalyst deactivation [18,39]. Smaller metal particle sizes increase the deactivation rate of the catalysts. This can be explained by the fact that CNTs are prone to form on a large particle when a smaller size is encapsulated by carbon [35].

Table 2. Different Ni and Ni/Cu catalysts on SiO₂ support and their effect on the carbon amounts and yields in the TCD reaction (at 1023 K and with GHSV of 1800).

Catalyst	Support	Operating Temperature [K]	GHSV [mL/g _{cat} h]	g _C /g _{CH₄} Fed	Carbon Yield %	Source
50 wt% Ni	SiO ₂	1023	1800	0.504	600%	
50 wt% Ni/5 wt% Cu	SiO ₂	1023	1800	0.531	610%	
50 wt% Ni/10 wt% Cu	SiO ₂	1023	1800	0.619	710%	[47]
50 wt% Ni/15 wt% Cu	SiO ₂	1023	1800	0.467	550%	
50 wt% Ni/20 wt% Cu	SiO ₂	1023	1800	0.374	500%	

Fe catalysts are cheaper and more environmentally friendly compared to Ni, although they require a somewhat higher temperature range [43]. Torres et al. [24] tested Fe catalysts with and without cobalt doping. Results indicated that cobalt-doped catalysts had higher carbon formation and longer activity. Both catalysts had an average diameter of around 12 nm. The difference was that the cobalt-doped catalyst had straighter CNTs than the iron catalyst. In addition, less metal was infused into the carbon with the cobalt-doped catalyst at 18.1 wt%, when the iron catalyst had 32.5 wt%. Carbon morphology can vary with the catalyst, as shown in Figure 4, which illustrates the carbons produced in the TCD process with iron and nickel catalysts. It can be seen that more nanotube-like carbon (a–c) is formed using the nickel catalyst, whereas the use of iron catalyst leads to the formation of more laminal (d–e) carbon.

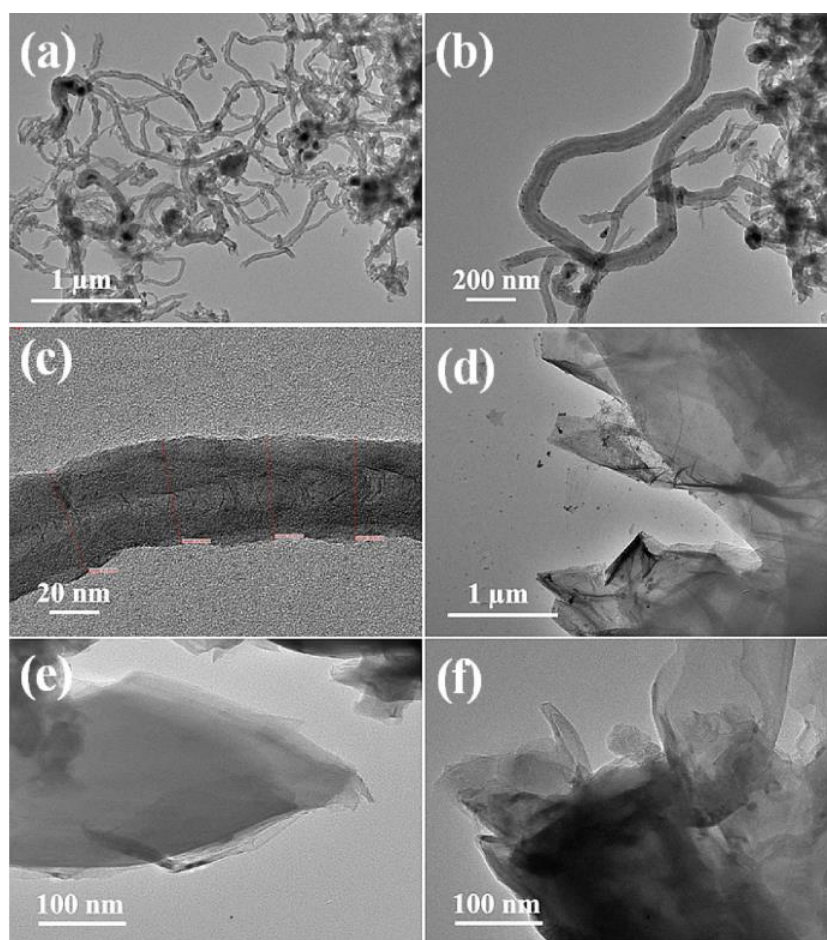


Figure 4. TEM images of the nanocarbon deposits using (a–c) Ni/MgO and (d–f) Fe/MgO catalysts [48]. Use of a nickel catalyst leads to nanotube-like carbon, whereas the use of an iron catalyst leads to the formation of more laminal carbon. Adapted with permission from [48]. Elsevier, 2017.

Other catalysts that have been investigated for TCD are molten metal catalysts and noble catalysts. The high cost of noble catalysts (Pt, Rh, Pd) prevents their use. Therefore, they are mostly used as a promoter to improve catalyst capability to produce carbon and thermal stability [45]. Takenaka et al. [49] studied the effect of different metals (Cu, Rh, Pd, Ir, and Pt) with nickel catalysts. The results indicated that a nickel catalyst with the addition of Pd significantly improved not only the catalytic life and hydrogen yield but also the carbon yield. Using a molten metal catalyst is one option to confront the issue of how to separate the produced carbon from the catalyst [50]. The idea is that solid carbon floats to the surface where it can be collected [37]. Guo et al. [51] studied the effect of support on the TCD process with mixed metal oxides (MMOs) and Al₂O₃. The results indicated that the MMOs resulted in a better hydrogen yield than Al₂O₃, but a lower carbon yield. The highest carbon yield, of 4.55 g_C/g_{Cat}, was obtained with a Ni₃Al catalyst. Ermakova and Ermakov [52] studied different types of support and their effect on the carbon yield. The highest yield of carbon (45 g_C/g_{Cat}) was obtained with SiO₂ support. Without any support, the carbon yield was 16.5 g_C/g_{Cat}, and with common Al₂O₃ support the carbon yield was 14 g_C/g_{Cat}. Awadallah et al. [27] studied the type of carbon that is formed on the catalyst with different supports. They used a Ni catalyst supported by zeolite samples with Si/Al ratios of 25 and 400 and amorphous silica. The Ni catalyst with zeolite 400 support yielded 372% of carbon, whereas with amorphous silica support the carbon yield was 9%. Zeolite samples formatted multiwalled CNTs in which amorphous silica formed graphene layers. They stated that this could be explained by the crystallite size of the Ni species and dispersion. Small crystallite size and high metal dispersion promote the growth of multiwalled CNTs. By comparison, lower dispersion and agglomerated Ni particles promote more horizontal growth to form graphene layers. Details of these studies can be found in Table 3, in which the type of catalyst and support, temperature, GHSV, and carbon yields are given.

Table 3. Different catalysts and supports, GHSV, and their effect on the carbon amounts and yields in the TCD reaction at 973 K.

Catalyst	Support	Operating Temperature [K]	GHSV [mL/g _{cat} h]	g _C /g _{Cat}	Carbon Yield %	Source
Ni _{0.5} Al (Molar ratio)	MMOs	973	60,000 *	0.11		
Ni ₁ Al	MMOs	973	60,000 *	0.49		
Ni ₂ Al	MMOs	973	60,000 *	2.02		
Ni ₃ Al	MMOs	973	60,000 *	4.55		[51]
Ni _{0.5}	Al ₂ O ₃	973	60,000 *	0.67		
Ni ₁	Al ₂ O ₃	973	60,000 *	1.15		
Ni ₂	Al ₂ O ₃	973	60,000 *	1.36		
Ni ₃	Al ₂ O ₃	973	60,000 *	1.29		
85wt% Fe	ZrO ₂	973	8000	13.5		
85wt% Fe	Al ₂ O ₃	973	8000	14		
85wt% Fe	TiO ₂	973	8000	17.4		[52]
85wt% Fe	SiO ₂	973	8000	45		
85wt% Fe	–	973	8000	16.5		
40 wt% Ni	Z-25	973	6000 *		176%	
40 wt% Ni	Z-400	973	6000 *		372%	[27]
40 wt% Ni	Amorphous silica	973	6000 *		9%	

* Calculated from flow rate to GHSV.

4.2. Effect of Process Temperature on Carbon Amount and Quality

Temperature can affect the BET surface and, according to Torres et al. [23], the BET value increases with the decrease in temperature. An increase in temperature can affect the amount of carbon formed [53]. It is also suggested that, to obtain higher crystallinity of carbon, higher reaction temperatures could be beneficial, but only up to a certain point.

Above 1473 K, carbon morphology is more amorphous [16,45]. In Table 4, two different studies are shown in which temperature was the variable in the TCD process. Table also shows the catalyst used and the corresponding process conditions. Carbon yields for each catalyst/support are also presented.

Table 4. The effect of temperature on carbon yield based on two different studies using Ni and Fe catalysts. As can be seen, the carbon yield increased with the increase in temperature.

Catalyst	Support	Operating Temperature [K]	GHSV [mL/g _{cat} h]	Carbon Yield %	Source
Ni	MgO	1173	9000 *	927%	[48]
Ni	MgO	1073	9000 *	863%	
Ni	MgO	973	9000 *	608%	
Fe	MgO	1173	9000 *	1205%	
Fe	MgO	1073	9000 *	1055%	
Fe	MgO	973	9000 *	810%	
NiO		1173	9000 *	815%	[54]
NiO		1073	9000 *	691%	
NiO		973	9000 *	341%	
Fe ₂ O ₃		1173	9000 *	663%	
Fe ₂ O ₃		1073	9000 *	419%	
Fe ₂ O ₃		973	9000 *	196%	

* Calculated from flow rate to GHSV.

In the research of Pudukudy et al. [48], the catalysts Ni and Fe were studied, based on MgO support at different temperatures. The Fe catalyst had a higher carbon yield at all temperatures than the Ni catalyst. With both catalysts, the carbon yield increased with the increase in temperature as can be seen in Table 4. In another study, Pudukudy et al. [54] investigated the effect of temperature on NiO and Fe₂O₃ catalysts, and its effect on the carbon yield. As the temperature increased, the carbon yield increased, and NiO had overall higher yields compared with Fe₂O₃. At 973 K, the carbon yields were 341% and 196% using NiO and Fe₂O₃ catalysts, respectively. At the highest reaction temperature, 1173 K, the carbon yields were 815% and 663% for NiO and Fe₂O₃ catalysts, respectively. In the studies of Takenaka et al. [41], temperature had the opposite effect. Carbon and hydrogen yields both decreased with the increase in the reaction temperature. They also found that at 773 K fish-bone type carbon fibers formed, whereas at 973 K they were mostly multiwalled CNTs (MWCNTs). Saraswat and Pant [47] showed that the carbon yield increased with increasing temperatures from 823 to 1023 K but decreased from 1023 to 1073 K. They used Ni and bimetallic catalysts with the support of zeolite MCM-22.

4.3. Effect of GHSV on Carbon Amount and Quality

Increasing the methane flow rate affects the deactivation rate and the carbon. According to Gao et al. [23], the carbon fiber is thicker and the BET decreases when the methane flow rate is increased.

Saraswat et al. [47] studied the effect of GHSV on methane conversion and carbon yield. They previously determined that the optimal catalyst and temperature were 50%Ni-10%Cu/SiO₂ at 1023 K. This combination resulted in the highest conversion rate. They then studied the influence of GHSV with different velocities ranging from 600 to 6000 mL/g_{cat}h. They found that the catalyst had the highest activity at 600 mL/g_{cat}h and, as the GHSV increased, both methane and carbon yields decreased. This suggests that, at a higher flow rate, the catalyst is covered with carbon deposits; therefore, by deactivating the catalyst and using lower flow rates, the decomposition reaction is more effective on the catalyst surface.

4.4. Summary

It is important to note that the reaction is affected by many parameters, and the results can vary significantly. It is crucial to identify the parameters that result in good carbon

yields without compromising the hydrogen yield. Table 5 summarizes TCD reactions with different process parameters, catalysts, and supports used, and their effect on the carbon amount and morphology. It should be noted that although researchers may report in their experiments that only one type of carbon is formed, all of the other carbon morphologies may also be present in the process; often, the dominant carbon or the form of carbon that is of most interest to the researcher is the only one reported.

Table 5. Other catalysts and supports used in the TCD process, operation conditions, and their effect on the produced carbon yield and morphology.

Catalyst	Support	Operating Temperature [K]	GHSV [mL/g _{cat} h]	Carbon Deposits [g _C /g _{cat}]	Carbon Morphology	Source
Fe (porous)		1173	9000	6.62	Layered graphene sheets	[55]
Ni		773	9000	354–398	CNT	[56]
40 wt% Ni	SiO ₂	773	90,000 *	491	Fish-bone carbon nanofibers	[41]
40 wt% Ni	SiO ₂	973	90,000 *		MWCNT	
75 wt% Ni	SiO ₂	823	30,000 *		Longer and thicker than at 923 K Thinner and shorter than without Fe	[57]
35 wt% Ni/40 wt% Fe	SiO ₂	823	30,000 *			
65 wt% Ni/10 wt% Fe	SiO ₂	823	30,000 *			
75 wt% Ni	SiO ₂	923	18,000 *			
35 wt% Ni/40 wt% Fe	SiO ₂	923	18,000 *			
65 wt% Ni/10 wt% Fe	SiO ₂	923	18,000 *			
50 wt% Ni/25 wt% Fe	Al ₂ O ₃	973	4200 *	562	CNT	[58]
50 wt% Ni	MCM-22	1023	1800	3.63	CNT	[38]
50 wt% Ni/5 wt% Cu	MCM-22	1023	1800	4.26	CNT	
50 wt% Ni/5 wt% Cu/5 wt% Zn	MCM-22	1023	1800	5.68	CNT	
50 wt% Ni/10 wt% Cu	MCM-22	1023	1800	5.5	CNT	
50 wt% Ni/10 wt% Zn	MCM-22	1023	1800	5.45	CNT	
5 wt% Ni	SiO ₂	873	2440	27.16 **	CNT	[59]
10 wt% Ni	SiO ₂	873	2440	39.73 **		
20 wt% Ni	SiO ₂	873	2440	57.94 **		
30 wt% Ni	SiO ₂	873	2440	62.05 **		
40 wt% Ni	SiO ₂	873	2440	35.99 **		
50 wt% Ni	SiO ₂	873	2440	23.91 **		
60 wt% Ni	SiO ₂	873	2440	16.54 **		
70 wt% Ni	SiO ₂	873	2440	9.01 **		
90 wt% Ni	SiO ₂	873	2440	1.00 **		
69 wt% Fe	Al ₂ O ₃	973	6000	2.28		[60]
69 wt% Fe	Al ₂ O ₃	1073	6000	4.25		
69 wt% Fe	Al ₂ O ₃	1123	6000	2.3		
69 wt% Fe	Al ₂ O ₃	1173	6000	3.02		
69 wt% Fe	Al ₂ O ₃	1073	3000	3.6		
69 wt% Fe	Al ₂ O ₃	1073	8000	4.8		
12.3Fe/1Mo/6.15Al ₂ O ₃ (molar ratio)	Al ₂ O ₃	1023	1500	1.92	bamboo shaped	[28]
50 wt%						
12.3Fe/1Mo/6.15MgO(molar ratio)	MgO	1023	1500	8.26	tubular	
8.6 wt% Ni	AC	1123	1620	7.01		[61]
16.6 wt% Ni	AC	1123	1620	9.23		
23.3 wt% Ni	AC	1123	1620	7.92		
30 wt% Ni	AC	1123	1620	6.10		
Graphitized carbon black (Carbopack C)		1123	3800	0.08		[62]
Graphitized carbon black (Carbopack B)		1123	3800	0.12		
Carbon black (Fluke 05120)		1123	3800	0.65		
Carbon black (Fluka 05120)		1123	9500	0.69		
Carbon black (Fluka 03866)		1123	3800	0.212		
Carbon black (Black pearls 2000)		1123	3800	0.22		
Industrial carbon black (HS-50)		1123	3800	0.28		
Commercial activated carbon (CGNorit)		1123	3800	0.45		
Commercial activated carbon (CGNorit)		1123	9500	0.6		
Commercial activated carbon (CGNorit)		1123	19,000	0.66		
26.5 wt% Fe	SiO ₂	1073	105,000	7.5	CNT	[63]
26.5 wt% Fe	SiO ₂	1073	105,000	22.5	CNT	
90 wt% Fe	Al ₂ O ₃	898	45,000	5.5		[64]
85 wt% Fe/5 wt% Co	Al ₂ O ₃	823	45,000	16		
50 wt% Fe	Al ₂ O ₃	823	45,000	26.5		
50 wt% Fe/6 wt% Co	Al ₂ O ₃	823	45,000	52.4		

* Calculated from flow rate to GHSV. ** Calculated from mol_C/mol_{Ni} to g_C/g_{Ni}.

5. Possible Applications for Produced Solid Carbon

Demand for carbon products is expected to grow in the future [24]. Currently, the most common production methods are plasma arc discharge, pulsed laser gasification, and catalytic chemical vapor deposition. The first of these has a high operation temperature of 4000–6000 K, and the latter has normal pressure and a temperature of 800–1200 K. In TCD, both products' hydrogen and carbon may be valuable in the future; therefore, there is significant interest in the process and applications for produced carbon. These applications vary depending on the type of carbon produced; for example, CNOs have been applied in lubrication oils and supercapacitors. CNTs have been used in water purification treatment and in conductive polymers [25,65].

In this article, we introduce possible applications in which carbon materials are currently being used or could be used. Not all of the studies relate to carbon materials manufactured by TCD. Nonetheless, this process has the potential to become economically feasible because, in many applications, increasing the scale of manufacturing is one of the biggest challenges [66]. It should be noted that, although many of these applications have been tested in the laboratory, they may not be ethically viable or safe for humans in practice; a good example is water purification, because carbon nanotubes are considered toxic to humans [67].

5.1. Batteries

Battery manufacturers continuously attempt to improve charging rate, energy density, operating temperature, power density, safety, energy density, and sufficient electrochemical cycling characteristics. Electrode materials play a key role in battery development. CNTs have been studied as an anode material for Li-ion batteries [68]. Traditionally, in Li-ion batteries, graphite has been used as the anode material because of its good electric conductivity. In high power applications, graphene is replaced with materials that have higher capacity, energy, and power density. CNT morphology, high conductivity and tensile strength, and inertness to chemical degradation can improve battery capacity and decrease the risk of pulverization as an anode material, and can therefore be considered as a replacement material for graphene. If CNTs are used in batteries, they should be free from contaminants, such as metal catalysts, amorphous carbon, fullerenes, and nanotubes with divergent morphology. Large-scale production is still under development and the prices remain relatively high.

5.2. Supercapacitors

TCD-produced carbon provides a less-expensive, environmentally friendly choice for supercapacitor materials, without compromising the material properties required [68]. Porous carbon materials are attractive materials for the production of electrodes due to their high thermal and chemical stability, good electrical conductivity, and porous structure. Optimal supercapacitor materials should have an accessible and high specific surface area in the microporous region. A certain balance should be obtained between the energy storage-related pores and interconnecting pores to achieve the best properties; therefore, the ability to control the porosity of the carbon by production parameters is crucial [31].

5.3. Water Treatment Application

Because CNTs have a relatively large specific surface area and a porous structure, they may be used as an absorbent of organic pollutants from wastewater [69,70]. Although CNTs show promise in this regard, a number of critical obstacles must first be overcome. First is the poor separability of the carbon and pollutant. Second is that studies have shown that CNTs' only have the ability to absorb a single organic pollutant, whereas wastewater can have several pollutants, such as metal ions, anions, humic acid, and organic solvents. Third is the economic issue. Thus, in the more practical applications of CNTs, more attention should be paid to finding means to make the operation more feasible for water treatment [71].

CNTs can also be toxic to the human body [72,73], and therefore, it should be carefully considered whether they should be applied to wastewater treatment.

5.4. Composite Materials

MWCNTs may be used as a composite material. Combined with polymers, several applications are possible [74]. This composite material may be used, for example, in wearable electronics in textile sectors [75], antennas [76], sensors [77], solar cells [78,79], and EMI shielding [80–83]. The use of these materials can also overcome existing challenges and allow industrialization of new applications, such as healthcare devices, packaging, and shield protection for humans. Previous studies have also noted that this type of composite material may replace steel in various appliances due to its superior electric conductivity.

5.5. Cosmetics and Medical Applications

Carbon-based nanoparticles are being used in cosmetics and medical applications. For example, fullerenes have potential in biomedicine because of their antioxidant activity. They show promise in dermatological and skin care products, such as sunscreen, skin whitening, and antiaging products [83]. Fullerenes can act as a vehicle to improve drug delivery and hair growth. Carbon black can be used as a colorant in cosmetic products, and activated carbon is used in toothpastes [80,81]. Charcoal has been used in medicine dating back to ancient Egyptian civilizations. Currently, charcoal is used for teeth whitening, smoothing the skin, facial cleansing, pore striping, facial masks, and soaps. It has been noted that it can treat acne, bites or cuts, minor infections, itchy scalp, and seborrheic dermatitis. Activated charcoal removes dirt, oil, and impurities, absorbs toxins, has antibacterial properties, tightens pores, smooths skin, reduces inflammation, and decongests and brightens the skin [82].

6. Conclusions

CO₂-free hydrogen production is a key area in the effort to achieve the EU's ambitious environmental and carbon neutrality goals. TCD, which is a CO₂-free process, may be used in the future to produce both hydrogen and solid carbon. In this article, we focused on the production of solid carbon, including its properties, the effect of the TCD process on its quality, and its possible applications. Carbon produced using TCD could have a significant effect on the hydrogen economy and increase the value added by the process. Compared to other methane-based hydrogen production processes, this carbon is bound in a solid form and can be used in carbon capture with zero CO₂ emissions.

Carbon can take several forms, such as graphene, diamond, fullerenes, and nanotubes. These different morphologies can have various properties and applications. Therefore, understanding the manufacturing process and parameter effects is crucial to obtain the quality that is desired for the application. In the TCD catalyst, the promoter, temperature, and methane gas flow can influence the carbon type and quality.

Because carbon materials are currently widely used or studied for various applications, carbon manufactured by TCD could provide the impetus for its use in several application areas, such as batteries, supercapacitors, and composite material. This would increase their potential uses, and make them more economically friendly and feasible. However, in some applications, such as water purification, CNT toxicity to humans remains an issue that must be considered.

Author Contributions: Conceptualization, U.L., H.R., E.V. and L.Y.-V.; Writing—original draft preparation, E.V.; Writing—review and editing, U.L., H.R., E.V. and L.Y.-V.; visualization, U.L., H.R.; supervision, U.L.; funding acquisition, E.V., U.L. and H.R. All authors have read and agreed to the published version of the manuscript.

Funding: This research was funded by the Fortum and Neste Foundation, grant number 20200148.

Institutional Review Board Statement: Not applicable.

Informed Consent Statement: Not applicable.

Conflicts of Interest: The authors declare no conflict of interest in regard to this work.

References

1. European Commission. *A Hydrogen Strategy for a Climate-Neutral Europe*; European Commission: Brussels, Belgium, 2020.
2. Yang, L.; Liu, F.; He, J. Natural Sand as a Non-Conventional Catalyst for Hydrogen Production by Methane Thermo-Catalytic Decomposition. *Int. J. Hydrogen Energy* **2019**, *44*, 11625–11633. [[CrossRef](#)]
3. Gamal, A.; Eid, K.; El-Naas, M.H.; Kumar, D.; Kumar, A. Catalytic Methane Decomposition to Carbon Nanostructures and Cox-Free Hydrogen: A Mini-Review. *Nanomaterials* **2021**, *11*, 1226. [[CrossRef](#)] [[PubMed](#)]
4. Chen, L.; Qi, Z.; Zhang, S.; Su, J.; Somorjai, G.A. Catalytic Hydrogen Production from Methane: A Review on Recent Progress and Prospect. *Catalysts* **2020**, *10*, 858. [[CrossRef](#)]
5. Abbas, H.F.; Wan Daud, W.M.A. Hydrogen Production by Methane Decomposition: A Review. *Int. J. Hydrogen Energy* **2010**, *35*, 1160–1190. [[CrossRef](#)]
6. Abdullah, B.; Abd Ghani, N.A.; Vo, D.V.N. Recent Advances in Dry Reforming of Methane over Ni-Based Catalysts. *J. Clean. Prod.* **2017**, *162*, 170–185. [[CrossRef](#)]
7. Soltani, R.; Rosen, M.A.; Dincer, I. Assessment of CO₂ Capture Options from Various Points in Steam Methane Reforming for Hydrogen Production. *Int. J. Hydrogen Energy* **2014**, *39*, 20266–20275. [[CrossRef](#)]
8. Usman, M.; Wan Daud, W.M.A.; Abbas, H.F. Dry Reforming of Methane: Influence of Process Parameters—A Review. *Renew. Sustain. Energy Rev.* **2015**, *45*, 710–744. [[CrossRef](#)]
9. Levalley, T.L.; Richard, A.R.; Fan, M. The Progress in Water Gas Shift and Steam Reforming Hydrogen Production Technologies—A Review. *Int. J. Hydrogen Energy* **2014**, *39*, 16983–17000. [[CrossRef](#)]
10. Kumar, S.; Kumar, S.; Prajapati, J.K. Hydrogen Production by Partial Oxidation of Methane: Modeling and Simulation. *Int. J. Hydrogen Energy* **2009**, *34*, 6655–6668. [[CrossRef](#)]
11. De, C.; Roseno, K.T.; Schmal, M.; Brackmann, R.; Alves, R.M.B.; Giudici, R. Partial Oxidation of Methane on Neodymium and Lanthanum Chromate Based Perovskites for Hydrogen Production. *Int. J. Hydrogen Energy* **2019**, *44*, 8166–8177. [[CrossRef](#)]
12. Larimi, A.S.; Alavi, S.M. Ceria-Zirconia Supported Ni Catalysts for Partial Oxidation of Methane to Synthesis Gas. *Fuel* **2012**, *102*, 366–371. [[CrossRef](#)]
13. Ruckenstein, E.; Hu, Y.H. Methane Partial Oxidation over NiO/MgO Solid Solution Catalysts. *Appl. Catal. A Gen.* **1999**, *183*, 85–92. [[CrossRef](#)]
14. Ibrahim, A.A.; Al-Fatesh, A.S.; Khan, W.U.; Soliman, M.A.; Al Otaibi, R.L.; Fakeeha, A.H. Thermo-Catalytic Methane Decomposition: A Review of State of the Art of Catalysts. *J. Chem. Soc. Pakistan* **2015**, *37*, 1269–1297.
15. Ashik, U.P.M.; Wan Daud, W.M.A.; Abbas, H.F. Production of Greenhouse Gas Free Hydrogen by Thermocatalytic Decomposition of Methane—A Review. *Renew. Sustain. Energy Rev.* **2015**, *44*, 221–256. [[CrossRef](#)]
16. Keipi, T.; Tolvanen, K.E.S.; Tolvanen, H.; Konttinen, J. Thermo-Catalytic Decomposition of Methane: The Effect of Reaction Parameters on Process Design and the Utilization Possibilities of the Produced Carbon. *Energy Convers. Manag.* **2016**, *126*, 923–934. [[CrossRef](#)]
17. Pudukudy, M.; Yaakob, Z.; Akmal, Z.S. Direct Decomposition of Methane over SBA-15 Supported Ni, Co and Fe Based Bimetallic Catalysts. *Appl. Surf. Sci.* **2015**, *330*, 418–430. [[CrossRef](#)]
18. Liang, W.; Yan, H.; Chen, C.; Lin, D.; Tan, K.; Feng, X.; Liu, Y.; Chen, X.; Yang, C.; Shan, H. Revealing the Effect of Nickel Particle Size on Carbon Formation Type in the Methane Decomposition Reaction. *Catalysts* **2020**, *10*, 890. [[CrossRef](#)]
19. Zhou, L.; Enakonda, L.R.; Harb, M.; Saih, Y.; Aguilar-Tapia, A.; Ould-Chikh, S.; Hazemann, J.-L.; Li, J.; Wei, N.; Gary, D.; et al. Fe Catalysts for Methane Decomposition to Produce Hydrogen and Carbon Nano Materials. *Appl. Catal. B Environ.* **2017**, *208*, 44–59. [[CrossRef](#)]
20. Callister, W.D. *Materials Science and Engineering: An Introduction*, 7th ed.; John Wiley & Sons: New York, NY, USA, 2007.
21. Noked, M.; Soffer, A.; Arubach, D. The Electrochemistry of Activated Carbonaceous Materials: Past, Present, and Future. *J. Solid State Electrochem.* **2011**, *15*, 1563–1578. [[CrossRef](#)]
22. Qian, J.X.; Chen, T.W.; Enakonda, L.R.; Liu, D.B.; Basset, J.M.; Zhou, L. Methane Decomposition to Pure Hydrogen and Carbon Nano Materials: State-of-the-Art and Future Perspectives. *Int. J. Hydrogen Energy* **2020**, *45*, 15721–15743. [[CrossRef](#)]
23. Gao, L.Z.; Kiwi-Minsker, L.; Renken, A. Growth of Carbon Nanotubes and Microfibers over Stainless Steel Mesh by Cracking of Methane. *Surf. Coatings Technol.* **2008**, *202*, 3029–3042. [[CrossRef](#)]
24. Torres, D.; Pinilla, J.L.; Suelves, I. Cobalt Doping of α -Fe/Al₂O₃ Catalysts for the Production of Hydrogen and High-Quality Carbon Nanotubes by Thermal Decomposition of Methane. *Int. J. Hydrogen Energy* **2020**, *45*, 19313–19323. [[CrossRef](#)]
25. Liu, Q.; Wu, P.; He, J.; Liu, C.; Jiang, W. Catalytic Decomposition of Methane by Two-Step Cascade Catalytic Process: Simultaneous Production of Hydrogen and Carbon Nanotubes. *Chem. Eng. Res. Des.* **2020**, *163*, 96–106. [[CrossRef](#)]
26. Soni, S.K.; Thomas, B.; Kar, V.R. A Comprehensive Review on CNTs and CNT-Reinforced Composites: Syntheses, Characteristics and Applications. *Mater. Today Commun.* **2020**, *25*, 101546. [[CrossRef](#)]
27. Awadallah, A.E.; El-Desouki, D.S.; Aboul-Gheit, N.A.K.; Ibrahim, A.H.; Aboul-Gheit, A.K. Effect of Crystalline Structure and Pore Geometry of Silica Based Supported Materials on the Catalytic Behavior of Metallic Nickel Particles during Methane Decomposition to CO_x-Free Hydrogen and Carbon Nanomaterials. *Int. J. Hydrogen Energy* **2016**, *41*, 16890–16902. [[CrossRef](#)]

28. Torres, D.; Pinilla, J.L.; Lázaro, M.J.; Moliner, R.; Suelves, I. Hydrogen and Multiwall Carbon Nanotubes Production by Catalytic Decomposition of Methane: Thermogravimetric Analysis and Scaling-up of Fe-Mo Catalysts. *Int. J. Hydrogen Energy* **2014**, *39*, 3698–3709. [[CrossRef](#)]
29. Williams, P.T. Hydrogen and Carbon Nanotubes from Pyrolysis-Catalysis of Waste Plastics: A Review. *Waste Biomass Valorization* **2020**, *12*, 1–28. [[CrossRef](#)]
30. Dagle, R.; Dagle, V.; Bearden, M.; Holladay, J.; Krause, T.; Ahmed, S. *R & D Opportunities for Development of Natural Gas Conversion Technologies for Co-Production of Hydrogen and Value-Added Solid Carbon Products*; U.S. Department of Energy Fuel Cell Technologies Office: Chicago, IL, USA, 2017.
31. Gu, W.; Yushin, G. Review of Nanostructured Carbon Materials for Electrochemical Capacitor Applications: Advantages and Limitations of Activated Carbon, Carbide-Derived Carbon, Zeolite-Templated Carbon, Carbon Aerogels, Carbon Nanotubes, Onion-like Carbon, and Graphene. *Wiley Interdiscip. Rev. Energy Environ.* **2014**, *3*, 424–473. [[CrossRef](#)]
32. Han, F.D.; Yao, B.; Bai, Y.J. Preparation of Carbon Nano-Onions and Their Application as Anode Materials for Rechargeable Lithium-Ion Batteries. *J. Phys. Chem. C* **2011**, *115*, 8923–8927. [[CrossRef](#)]
33. Bai, Z.; Chen, H.; Li, B.; Li, W. Methane Decomposition over Ni Loaded Activated Carbon for Hydrogen Production and the Formation of Filamentous Carbon. *Int. J. Hydrogen Energy* **2007**, *32*, 32–37. [[CrossRef](#)]
34. Lobo, L.S.; Carabineiro, S.A.C. Carbon Formation at High Temperatures. *Catalysts* **2020**, *10*, 465. [[CrossRef](#)]
35. Guizani, C.; Escudero Sanz, F.J.; Salvador, S. The Nature of the Deposited Carbon at Methane Cracking over a Nickel Loaded Wood-Char. *Comptes Rendus Chim.* **2016**, *19*, 423–432. [[CrossRef](#)]
36. Torres, D.; Pinilla, J.L.; Suelves, I. Co-, Cu- and Fe-Doped Ni/Al₂O₃ Catalysts for the Catalytic Decomposition of Methane into Hydrogen and Carbon Nanofibers. *Catalysts* **2018**, *8*, 300. [[CrossRef](#)]
37. Upham, D.C.; Agarwal, V.; Khechfe, A.; Snodgrass, Z.R.; Gordon, M.J.; Metiu, H.; McFarland, E.W. Catalytic Molten Metals for the Direct Conversion of Methane to Hydrogen and Separable Carbon. *Science* **2017**, *358*, 917–921. [[CrossRef](#)]
38. Saraswat, S.K.; Pant, K.K. Ni-Cu-Zn/MCM-22 Catalysts for Simultaneous Production of Hydrogen and Multiwall Carbon Nanotubes via Thermo-Catalytic Decomposition of Methane. *Int. J. Hydrogen Energy* **2011**, *36*, 13352–13360. [[CrossRef](#)]
39. Christensen, K.O.; Chen, D.; Lødeng, R.; Holmen, A. Effect of Supports and Ni Crystal Size on Carbon Formation and Sintering during Steam Methane Reforming. *Appl. Catal. A Gen.* **2006**, *314*, 9–22. [[CrossRef](#)]
40. Hasnan, N.S.N.; Timmiati, S.N.; Lim, K.L.; Yaakob, Z.; Kamaruddin, N.H.N.; Teh, L.P. Recent Developments in Methane Decomposition over Heterogeneous Catalysts: An Overview. *Mater. Renew. Sustain. Energy* **2020**, *9*, 3. [[CrossRef](#)]
41. Takenaka, S.; Kobayashi, S.; Ogiwara, H.; Otsuka, K. Ni/SiO₂ Catalyst Effective for Methane Decomposition into Hydrogen and Carbon Nanofiber. *J. Catal.* **2003**, *217*, 79–87. [[CrossRef](#)]
42. Marquardt, T.; Bode, A.; Kabelac, S. Hydrogen Production by Methane Decomposition: Analysis of Thermodynamic Carbon Properties and Process Evaluation. *Energy Convers. Manag.* **2020**, *221*. [[CrossRef](#)]
43. Guil-Lopez, R.; Botas, J.A.; Fierro, J.L.G.; Serrano, D.P. Comparison of Metal and Carbon Catalysts for Hydrogen Production by Methane Decomposition. *Appl. Catal. A Gen.* **2011**, *396*, 40–51. [[CrossRef](#)]
44. Muradov, N.; Smith, F.; T-Raissi, A. Catalytic Activity of Carbons for Methane Decomposition Reaction. *Catal. Today* **2005**, *102–103*, 225–233. [[CrossRef](#)]
45. Ahmed, S.; Aitani, A.; Rahman, F.; Al-Dawood, A.; Al-Muhaish, F. Decomposition of Hydrocarbons to Hydrogen and Carbon. *Appl. Catal. A Gen.* **2009**, *359*, 1–24. [[CrossRef](#)]
46. Qian, J.X.; Chen, T.W.; Enakonda, L.R.; Liu, D.B.; Mignani, G.; Basset, J.M.; Zhou, L. Methane Decomposition to Produce CO_x-Free Hydrogen and Nano-Carbon over Metal Catalysts: A Review. *Int. J. Hydrogen Energy* **2020**, *45*, 7981–8001. [[CrossRef](#)]
47. Saraswat, S.K.; Pant, K.K. Synthesis of Hydrogen and Carbon Nanotubes over Copper Promoted Ni/SiO₂ Catalyst by Thermocatalytic Decomposition of Methane. *J. Nat. Gas Sci. Eng.* **2013**, *13*, 52–59. [[CrossRef](#)]
48. Pudukudy, M.; Yaakob, Z.; Mazuki, M.Z.; Takriff, M.S.; Jahaya, S.S. One-Pot Sol-Gel Synthesis of MgO Nanoparticles Supported Nickel and Iron Catalysts for Undiluted Methane Decomposition into CO_x Free Hydrogen and Nanocarbon. *Appl. Catal. B Environ.* **2017**, *218*, 298–316. [[CrossRef](#)]
49. Takenaka, S.; Shigeta, Y.; Tanabe, E.; Otsuka, K. Methane Decomposition into Hydrogen and Carbon Nanofibers over Supported Pd-Ni Catalysts. *J. Catal.* **2003**, *220*, 468–477. [[CrossRef](#)]
50. Munera Parra, A.A.; Agar, D.W. Molten Metal Capillary Reactor for the High-Temperature Pyrolysis of Methane. *Int. J. Hydrogen Energy* **2017**, *42*, 13641–13648. [[CrossRef](#)]
51. Guo, Z.; Zheng, J.E.; Liu, Y.; Chu, W. Insight into the Role of Metal/Oxide Interaction and Ni Availabilities on NiAl Mixed Metal Oxide Catalysts for Methane Decomposition. *Appl. Catal. A Gen.* **2018**, *555*, 1–11. [[CrossRef](#)]
52. Ermakova, M.A.; Ermakov, D.Y. Ni/SiO₂ and Fe/SiO₂ Catalysts for Production of Hydrogen and Filamentous Carbon via Methane Decomposition. *Catal. Today* **2002**, *77*, 225–235. [[CrossRef](#)]
53. Inaba, M.; Zhang, Z.; Matsuoka, K.; Soneda, Y. Optimization of the Reaction Conditions for Fe-Catalyzed Decomposition of Methane and Characterization of the Produced Nanocarbon Fibers. *Catal. Today* **2019**, *332*, 11–19. [[CrossRef](#)]
54. Pudukudy, M.; Yaakob, Z.; Dahani, N.; Takriff, M.S.; Hassan, N.S.M. Production of CO_x Free Hydrogen and Nanocarbon via Methane Decomposition Over Unsupported Porous Nickel and Iron Catalysts. *J. Clust. Sci.* **2017**, *28*, 1579–1594. [[CrossRef](#)]

55. Pudukudy, M.; Yaakob, Z.; Kadier, A.; Takriff, M.S.; Hassan, N.S.M. One-Pot Sol–Gel Synthesis of Ni/TiO₂ Catalysts for Methane Decomposition into CO_x Free Hydrogen and Multiwalled Carbon Nanotubes. *Int. J. Hydrogen Energy* **2017**, *42*, 16495–16513. [[CrossRef](#)]
56. Li, Y.; Zhang, B.; Xie, X.; Liu, J.; Xu, Y.; Shen, W. Novel Ni Catalysts for Methane Decomposition to Hydrogen and Carbon Nanofibers. *J. Catal.* **2006**, *238*, 412–424. [[CrossRef](#)]
57. Wang, W.; Wang, H.; Yang, Y.; Jiang, S. Ni-SiO₂ and Ni-Fe-SiO₂ Catalysts for Methane Decomposition to Prepare Hydrogen and Carbon Filaments. *Int. J. Hydrogen Energy* **2012**, *37*, 9058–9066. [[CrossRef](#)]
58. Wang, G.; Jin, Y.; Liu, G.; Li, Y. Production of Hydrogen and Nanocarbon from Catalytic Decomposition of Methane over a Ni-Fe/Al₂O₃ Catalyst. *Energy Fuels* **2013**, *27*, 4448–4456. [[CrossRef](#)]
59. Venugopal, A.; Naveen Kumar, S.; Ashok, J.; Hari Prasad, D.; Durga Kumari, V.; Prasad, K.B.S.; Subrahmanyam, M. Hydrogen Production by Catalytic Decomposition of Methane over Ni/SiO₂. *Int. J. Hydrogen Energy* **2007**, *32*, 1782–1788. [[CrossRef](#)]
60. Torres, D.; De Llobet, S.; Pinilla, J.L.; Lázaro, M.J.; Suelves, I.; Moliner, R. Hydrogen Production by Catalytic Decomposition of Methane Using a Fe-Based Catalyst in a Fluidized Bed Reactor. *J. Nat. Gas Chem.* **2012**, *21*, 367–373. [[CrossRef](#)]
61. Sarada Prasad, J.; Dhand, V.; Himabindu, V.; Anjaneyulu, Y. Production of Hydrogen and Carbon Nanofibers through the Decomposition of Methane over Activated Carbon Supported Ni Catalysts. *Int. J. Hydrogen Energy* **2011**, *36*, 11702–11711. [[CrossRef](#)]
62. Suelves, I.; Lázaro, M.J.; Moliner, R.; Pinilla, J.L.; Cubero, H. Hydrogen Production by Methane Decarbonization: Carbonaceous Catalysts. *Int. J. Hydrogen Energy* **2007**, *32*, 3320–3326. [[CrossRef](#)]
63. Takenaka, S.; Serizawa, M.; Otsuka, K. Formation of Filamentous Carbons over Supported Fe Catalysts through Methane Decomposition. *J. Catal.* **2004**, *222*, 520–531. [[CrossRef](#)]
64. Avdeeva, L.B.; Reshетенko, T.V.; Ismagilov, Z.R.; Likhoholov, V.A. Iron-Containing Catalysts of Methane Decomposition: Accumulation of Filamentous Carbon. *Appl. Catal. A Gen.* **2002**, *228*, 53–63. [[CrossRef](#)]
65. Fau, G.; Gascoin, N.; Gillard, P.; Steelant, J. Methane Pyrolysis: Literature Survey and Comparisons of Available Data for Use in Numerical Simulations. *J. Anal. Appl. Pyrolysis* **2013**, *104*, 1–9. [[CrossRef](#)]
66. Rashed, A.O.; Merenda, A.; Kondo, T.; Lima, M.; Razal, J.; Kong, L.; Huynh, C.; Dumée, L.F. Carbon Nanotube Membranes—Strategies and Challenges towards Scalable Manufacturing and Practical Separation Applications. *Sep. Purif. Technol.* **2021**, *257*, 117929. [[CrossRef](#)]
67. Ahmad, J.; Naeem, S.; Ahmad, M.; Usman, A.R.A.; Al-Wabel, M.I. A Critical Review on Organic Micropollutants Contamination in Wastewater and Removal through Carbon Nanotubes. *J. Environ. Manag.* **2019**, *246*, 214–228. [[CrossRef](#)] [[PubMed](#)]
68. Maziarka, P.; Sommersacher, P.; Wang, X.; Kienzl, N.; Retschitzegger, S.; Prins, W.; Hedin, N.; Ronsse, F. Tailoring of the Pore Structures of Wood Pyrolysis Chars for Potential Use in Energy Storage Applications. *Appl. Energy* **2021**, *286*, 116431. [[CrossRef](#)]
69. Peng, X.; Li, Y.; Luan, Z.; Di, Z.; Wang, H.; Tian, B.; Jia, Z. Adsorption of 1,2-Dichlorobenzene from Water to Carbon Nanotubes. *Chem. Phys. Lett.* **2003**, *376*, 154–158. [[CrossRef](#)]
70. Avci, A.; İnci, İ.; Baylan, N. Adsorption of Ciprofloxacin Hydrochloride on Multiwall Carbon Nanotube. *J. Mol. Struct.* **2020**, *1206*, 127711. [[CrossRef](#)]
71. Peng, J.; He, Y.; Zhou, C.; Su, S.; Lai, B. The Carbon Nanotubes-Based Materials and Their Applications for Organic Pollutant Removal: A Critical Review. *Chin. Chem. Lett.* **2021**. [[CrossRef](#)]
72. Mohanta, D.; Patnaik, S.; Sood, S.; Das, N. Carbon Nanotubes: Evaluation of Toxicity at Biointerfaces. *J. Pharm. Anal.* **2019**, *9*, 293–300. [[CrossRef](#)]
73. Keipi, T.; Hankalin, V.; Nummelin, J.; Raiko, R. Techno-Economic Analysis of Four Concepts for Thermal Decomposition of Methane: Reduction of CO₂ Emissions in Natural Gas Combustion. *Energy Convers. Manag.* **2016**, *110*, 1–12. [[CrossRef](#)]
74. Dhineshababu, N.R.; Mahadevi, N.; Assein, D. Electronic Applications of Multi-Walled Carbon Nanotubes in Polymers: A Short Review. *Mater. Today Proc.* **2020**. [[CrossRef](#)]
75. Wang, X.; Yang, B.; Liu, J.; Zhu, Y.; Yang, C.; He, Q. A Flexible Triboelectric-Piezoelectric Hybrid Nanogenerator Based on P(VDF-TrFE) Nanofibers and PDMS/MWCNT for Wearable Devices. *Sci. Rep.* **2016**, *6*. [[CrossRef](#)]
76. Zahir, H.; Wojkiewicz, J.; Alexander, P.; Kone, L.; Belkacem, B.; Bergheul, S.; Lasri, T. Design Fabrication and Characterisation of Polyaniline and Multiwall Carbon Nanotubes Composites-based Patch Antenna. *IET Microw. Antennas Propag.* **2016**, *10*, 88–93. [[CrossRef](#)]
77. Turkani, V.S.; Maddipatla, D.; Narakathu, B.B.; Saeed, T.S.; Obare, S.O.; Bazuin, B.J.; Atashbar, M.Z. A Highly Sensitive Printed Humidity Sensor Based on a Functionalized MWCNT/HEC Composite for Flexible Electronics Application. *Nanoscale Adv.* **2019**, *1*, 2311–2322. [[CrossRef](#)]
78. Kim, D.H.; Dudem, B.; Yu, J.S. High-Performance Flexible Piezoelectric-Assisted Triboelectric Hybrid Nanogenerator via Polydimethylsiloxane-Encapsulated Nanoflower-like ZnO Composite Films for Scavenging Energy from Daily Human Activities. *ACS Sustain. Chem. Eng.* **2018**, *6*, 8525–8535. [[CrossRef](#)]
79. Kar, E.; Bose, N.; Dutta, B.; Mukherjee, N.; Mukherjee, S. MWCNT@SiO₂ Heterogeneous Nanofiller-Based Polymer Composites: A Single Key to the High-Performance Piezoelectric Nanogenerator and X-Band Microwave Shield. *ACS Appl. Nano Mater.* **2018**, *1*, 4005–4018. [[CrossRef](#)]
80. Rincon, A.M. Chapter 6—Presence of nanomaterials on consumer products: Food, cosmetics, and drugs. In *Exposure to Engineered Nanomaterials in the Environment*; Elsevier: Amsterdam, The Netherlands, 2019; pp. 165–181, ISBN 9780128148365.

-
81. Viana, Í.E.L.; Weiss, G.S.; Sakae, L.O.; Niemeyer, S.H.; Borges, A.B.; Scaramucci, T. Activated Charcoal Toothpastes Do Not Increase Erosive Tooth Wear. *J. Dent.* **2021**, *109*, 103677. [[CrossRef](#)]
 82. Sanchez, N.; Fayne, R.; Burroway, B. Charcoal: An Ancient Material with a New Face. *Clin. Dermatol.* **2020**, *38*, 262–264. [[CrossRef](#)] [[PubMed](#)]
 83. Nafisi, S.; Maibach, H.I. Nanotechnology in cosmetics. In *Cosmetic Science and Technology: Theoretical Principles and Applications*; Elsevier: Amsterdam, The Netherlands, 2017; pp. 337–361, ISBN 9780128020548.